Proteomic profiling reveals engineered chitosan nanoparticles mediated cellular crosstalk and immunomodulation for therapeutic application in apical periodontitis

Hebatullah Hussein [a,b,c], Anil Kishen [a,b,d,e,*]

[a] *The Kishen Lab, Dental Research Institute, University of Toronto, Toronto, ON M5G 1G6, Canada*
[b] *Faculty of Dentistry, University of Toronto, Toronto, ON M5G 1G6, Canada*
[c] *Faculty of Dentistry, Ain Shams University, Endodontics Department, Cairo, Egypt*
[d] *School of Graduate Studies, University of Toronto, Toronto, ON M5G 1G6, Canada*
[e] *Department of Dentistry, Mount Sinai Health System, Mount Sinai Hospital, Toronto, ON M5G 1X5, Canada*

A R T I C L E   I N F O

A B S T R A C T

Macrophages (MQ) are major constituents of chronically inflamed periapical tissues in apical periodontitis. This study aimed to investigate the immunomodulatory effect of engineered bioactive chitosan-based nanoparticles (CSnp) antibiofilm medication on MQ cocultured with periodontal ligament fibroblasts (PdLF). Cells viability, spreading, PdLF migration, and intracellular CSnp uptake were characterized. Tandem Mass Tag-based proteomics was applied to analyze MQ global protein expression profiles after interaction with *Enterococcus faecalis* biofilm, CSnp-treated biofilm, and CSnp. Secreted inflammatory mediators were analyzed. Following bioinformatics analyses, candidate proteins were validated via targeted proteomics. CSnp maintained cells viability, increased MQ spreading, and PdLF migration ($p < 0.05$). Transmission electron micrographs demonstrated CSnp internalization via macropinocytosis, clathrin-mediated endocytosis, and phagocytosis. Proteomic analysis revealed that CSnp-treated biofilm upregulated proteins (>1.5-folds, $p < 0.05$) showed functional enrichment in the pathway of metal sequestration by antimicrobial proteins, while downregulated proteins showed enrichment in ferroptosis. CSnp upregulated proteins exhibiting antioxidant and immunoregulatory properties. Upregulation of *SERPINB1* by CSnp (>1.5-folds, $p < 0.05$) was validated. CSnp-treated biofilm reduced pro-inflammatory IL-1β and nitric oxide but enhanced anti-inflammatory IL-10 and TGF-β1 ($p < 0.05$). Internalized engineered bioactive CSnp reprogrammed MQ proteomic and cytokine profiles to modulate biofilm-mediated inflammation, and prompted PdLF migration, emphasizing its potential to regulate healing process in the treatment of apical periodontitis.

1. Introduction

A hallmark of chronic inflammation is the abundance of proinflammatory macrophages (MQ) in the inflamed tissue. MQ are activated by microbial ligands, cytokines, and growth factors, eliciting an immune response via different signaling pathways [1]. They consequently produce proinflammatory cytokines, reactive oxygen species (ROS), and nitrogen intermediates (M1). Activated MQ have been considered the main source for several cytokines involved in bone resorption, pathogenesis, and progression of apical periodontitis (AP), an inflammatory disorder of periradicular tissues caused primarily by bacteria organized as biofilm within root canal system [2,3]. Alternatively, under favorable stimuli, MQ produce anti-inflammatory cytokines facilitating periapical tissue healing (M2).

Half of the global adult population have at least one tooth with AP [4], a localized disease which could influence the systemic health of individuals [5]. An overall prevalence of AP in 59.45% of root-filled teeth has been reported [6]. Therefore, for a more predictable treatment outcome, it would benefit to modify the microenvironment to be conducive to periapical tissue healing, while effectively reducing intracanal biofilm. Since MQ play major role in providing a pro-regenerative niche, designing therapeutics to regulate MQ phenotype has been proposed to promote regeneration [7]. To the best of our

Abbreviations

AP	apical periodontitis
CS	chitosan
CSnp	chitosan-based nanoparticles
CMCS	carboxymethyl chitosan
COX	cyclo-oxygenase
CTSG	cathepsin-G
CYB5R1	cytochrome B5 reductase 1
C1QBP	C1q binding protein
DEP	differentially expressed proteins
DMEM	Dulbecco's Modified Eagle Medium
E. faecalis	*Enterococcus faecalis*
GO	Gene Ontology
IL	interleukin
KEGG	Kyoto Encyclopedia of Genes and Genomes
LC	liquid chromatography
MQ	macrophage
MIF	macrophage migration inhibitory factor
MS	mass spectrometry
MTT	3-(4,5-Dimethylthiazol-2-yl)-2,5-Diphenyltetrazolium Bromide
NAMPT	Nicotinamide phosphoribosyl-transferase
NO	nitric oxide
NF-κB	Nuclear Factor-kappa-B
PBS	phosphate-buffered saline
PCA	principal component analysis
PdLF	periodontal ligament fibroblast
PRDX1	Peroxiredoxin-1
PTMA	prothymosin alpha
PTGS1	prostaglandin G/H synthase 1
PRM	parallel reaction monitoring
ROS	reactive oxygen species
RPMI	Roswell Park Memorial Institute
SERPINB1	leukocyte elastase inhibitor
SOD1	Superoxide dismutase [Cu–Zn]
SOD2	Superoxide dismutase [Mn]
STRING	Search Tool for the Retrieval of Interacting Genes
TEM	transmission electron microscope
TGF	transforming growth factor
TLR	toll-like receptor
TMT	tandem mass tag
TNF	tumor necrosis factor
TXN	thioredoxin

knowledge, no endodontic medication has been assessed in terms of its modulatory effect on host immune cells at the protein level.

Naturally derived biomaterials with ROS-scavenging activities, could exhibit intrinsic anti-inflammatory effects [8]. Biopolymeric materials such as chitosan have been applied for periodontal regeneration [9]. Chitosan (CS)-based materials offer wide range of applications due to their bioactivity, biocompatibility, and biodegradability [10]. CS has excellent antimicrobial activities involving interaction between positively charged CS and negatively charged bacterial cell which affects bacterial cell permeability leading to leakage of intracellular components and cell death [11]. CS could provoke various cytokines of pro- or anti-inflammatory nature, based on many parameters including its structure, degree of deacetylation, molecular weight, and dose [12].

Engineered bioactive chitosan-based nanoparticles (CSnp) have been shown to possess an increased affinity to bacterial cell membrane, higher penetration into biofilm structure, and thus present a potential antimicrobial agent for root canal disinfection [13]. CSnp dispersed in a chitosan derivative, carboxymethyl chitosan (CMCS), have been employed as intracanal antibiofilm medication to dampen post-treatment MQ proinflammatory response [14,15]. They influenced the inflammatory reaction of MQ by virtue of their cationic charge, hydrophilicity, chemical moieties including the number of carboxyl, hydroxyl, and amino groups as well as their nanosized spherical structure. Therefore, the ability of CSnp to concurrently inactivate bacterial biofilm and modulate inflammatory response has the potential to harness its overall effect towards healing.

In nanoparticle-enabled immunomodulation, manipulating the particle's size and physicochemical characteristics can influence interaction with immune cells to induce the desired therapeutic benefit [16]. The uptake of nanoparticles is highly dependent on their intrinsic and extrinsic properties and would affect the biological functions of target cells. Mass spectrometry (MS)-based proteomics allow for accurate spatiotemporal identification and quantification of expressed proteins in a biological system, to achieve a comprehensive understanding of the cell's response to a wide range of stimuli [17]. The purpose of this study was to elucidate the mechanism by which CSnp modulates MQ inflammatory response to biofilm-mediated infection via MS-based proteomics and cytokine analyses using MQ-periodontal ligament fibroblast coculture system after characterizing cellular uptake and interaction with CSnp. Revealing the molecular mechanisms involved in engineered

antibacterial CSnp-mediated modulation of MQ could contribute to optimization of endodontic treatment through regulating periapical healing.

2. Materials and methods

All the chemicals used in this study were of analytic grade (purity ≥95%) and were purchased from Sigma-Aldrich Inc (St. Louis, MO, USA) unless otherwise stated. This study was approved by the University Ethics Review Board (protocol reference #35228). CSnp, previously synthesized and characterized [13,18,19], were prepared using the ionic gelation method as described earlier [20]. Chitosan was dissolved in 1 v/v% acetic acid solution at a concentration of 0.1 w/v%, followed by adjusting pH to 5 using 1 mol/L NaOH. Sodium tripolyphosphate in water (0.1%) was added to chitosan solution in a ratio of 3:1 under stirring at a speed of 1000 rpm to form CSnp which were separated by centrifugation at 15,000 rpm for 30 min. After discarding the supernatant, CSnp were thoroughly rinsed with deionized water to remove any residual NaOH and then freeze-dried [18]. CSnp were dispersed in 1% CMCS (1 mg/mL) [19].

2.1. Cell cultures and biofilm development

THP-1 monocytes (ATCC TIB-202, American Type Culture Collection, Manassas, VA, USA) cultured in RPMI1640, supplemented with 10% heat-inactivated fetal bovine serum (HIFBS), 1% Penicillin/Streptomycin and 0.05 mM 2-mercaptoethanol were differentiated with 100 nM phorbol 12-myristate 13-acetate (PMA) for 24h at 37 °C, 5% CO_2. Cells attachment and MQ-like morphology were confirmed. MQ were incubated for 16h in PMA-free culture media to rest.

Human periodontal ligament fibroblasts (PdLF), were cultured in DMEM supplemented with 10% HIFBS, 1% Penicillin/Streptomycin in humidified incubator at 37 °C, 5% CO_2 [21]. After 85% confluence, PdLF were detached with trypsin/EDTA 0.05% (Gibco, Canada) for 3min at 37 °C. Cells of third to fifth passage were used.

An overnight culture of **Enterococcus faecalis** (ATCC 29212, Manassas, VA, USA) in brain heart infusion broth ($OD_{600nm} = 1$) was incubated at 37 °C for 3 days in 24-well plates. The media was replenished after 48h. This protocol allowed the formation of abundant biofilm with a uniformly thick structure and complex matrix.

2.2. Cells characterization in the presence of CSnp

MQ and PdLF were characterized after interaction with CSnp regarding cell viability, spreading, PdLF cytoskeleton, and migration (details in supplementary material). The cells spreading area was assessed by thresholding the stained cells in the microscopic fields using ImageJ software (U.S. National Institutes of Health, Bethesda, Maryland, USA).

2.3. Intracellular uptake and trafficking of CSnp

Transmission electron microscopy (TEM) was used to image the cells after incubation with CSnp in serum-free DMEM for 3 and 24h, for qualitative assessment of CSnp cellular uptake pathways and visualization of CSnp intracellularly [22]. MQ (2x10ˆ6 cells/60 mm-plate) and PdLF (3x10ˆ5 cells/35 mm-plate) were detached using EDTA (1 mM) plus scrapping and trypsin/EDTA respectively. Cells were centrifuged, washed in PBS, and then fixed with 2.5% glutaraldehyde at 4 °C for 24h. After washing, the fixed samples were embedded in agar then postfixed with 1% osmium tetroxide for 1h. Samples were dehydrated in a graded series of ethanol and embedded in Spurr's resin. Embedded samples were stained with 1% UranyLess (EMS, Catalog #22409) and lead citrate. The 100 nm thick sections were placed on copper grids and examined under TEM (Hitachi HT-7700, Tokyo) at 80 kV.

2.4. Global protein expression profiles of differentiated macrophages

In transwell setup, differentiated MQ (1x10ˆ6 cells/well) were cocultured in 6-well plates with PdLF (1x10ˆ5 cells/insert) on the membrane (24 mm diameter; 8 μm pore size polycarbonate membrane, Corning, Lowell, MA). Antibiotic and serum-free DMEM were conditioned with: **(1) Biofilm**, untreated as positive control, **(2) CSnp-treated biofilm**, biofilm was treated by application of CSnp (1 mg/mL, 1mL/well) for 48h, and **(3) CSnp**, (1 mg/mL). Uninfected/non-treated cells, served as negative control **(Control)**. Conditioned media were applied to MQ-PdLF cocultures (5mL/well). After interaction for 3 and 24h, MQ cell lysates were prepared using RIPA buffer (Cell Signaling Technologies, Massachusetts, USA) with protease inhibitor cocktail. Protein concentration of lysates was determined using Bradford reagent (Bioshop, Canada). Lysates were dried down, reduced then alkylated. Samples were precipitated with acetone, centrifuged, and the pellet was dried. Peptide concentration was determined by A205 Scopes method (NanoDrop One, Thermo Scientific, USA) and 75 μg of protein was digested with Trypsin-LysC (Promega, USA).

2.4.1. Tandem mass tag (TMT) MS-based quantitative proteomics

Digested samples were labeled with TMT Label Reagent (Thermo-Fisher Scientific, USA). Peptides were purified, lyophilized (Speedvac, ThermoFisher Scientific, USA), and stored at −80 °C. Samples were analyzed on an Orbitrap Fusion Lumos Tribrid mass spectrometer equipped with nanospray source and nano-liquid chromatography (nano-LC) system (ThermoFisher, San Jose, CA, USA). MS data were acquired using MultiNotch synchronous precursor selection MS3 scanning for TMT tags. Proteome Discoverer 2.2 (ThermoFisher Scientific, USA) was used to analyze raw files and Uniprot human database (Uniprot-Human-Jan 15, 2018.fasta, Sequest HT) was searched for fragment lists, with parent and fragment mass tolerances set to 10 ppm and 0.6Da, respectively. Complete tryptic peptides with a maximum of two missed cleavages were accepted. Search results were filtered at the peptide spectral match level using a strict false discovery rate (FDR) q-value of 0.01 and relaxed FDR q-value of 0.05 [23]. TMT reporter ions were quantified.

2.4.2. Bioinformatics analyses

Proteins identified with at least 2 unique peptides and detected in two biological replicates of at least one group were included [24].

Identified proteins were analyzed against the non-redundant protein database using Gene Ontology (GO) analysis [25,26]. Protein encoding genes were categorized based on the biological process, molecular activity, and cellular components by the PANTHER gene classification system [27]. The proteins fold changes were calculated by comparing the normalized abundances among experimental groups relative to the control. Relative abundance with ratios of 'Divide 0' was replaced with the arbitrary number '10' in case the protein was not detected in the control group [28]. Heatmaps to visualize the hierarchical clustering of proteomics data and principal component analysis (PCA) were plotted using GENE.E [29] and BioVinci 2.0 (https://vinci.bioturing.com) respectively. Volcano plots depicting the magnitude of protein abundance change expressed as $\log_2$ of the fold change on the x-axis and minus $\log_{10}$ of the P-value on the y-axis were constructed using Prism v8.0.0 (GraphPad, San Diego, CA, USA). Identified proteins with P-values ≤ 0.05 and fold changes ≥ 1.5 compared to the control were considered as differentially expressed proteins (DEP). Protein-protein interaction networks of the DEP at 24h were analyzed using STRING-v11.0 (Search Tool for the Retrieval of Interacting Genes) [30]. Proteins abundance was compared between CSnp-treated biofilm and untreated biofilm and graphs of selected proteins were plotted.

2.5. Validation of candidate proteins

Five of the DEPs in the 24h data set were validated across samples using parallel reaction monitoring (PRM)- targeted MS. Using an S-trap protocol, the cell lysates were reduced, alkylated, then digested with trypsin (Pierce, 2h at 37 °C on-column). Eluted peptides were dried and stored at −20 °C. After quantifying the peptides, PRM method was developed using the control sample. A discovery LC-MS/MS run was completed to determine the suitable peptides followed by 3 runs to fine-tune them. Appropriate peptides were selected using Skyline software and their precursor masses were used as targeted m/z. The most suitable fragment ions for each peptide were chosen for quantitative measurement, where 2ug of peptides/sample were run for 1h. Results were analyzed in Skyline software and peaks for each set of fragment ions were manually checked to ensure the peak boundaries were correct. The area under the curve for each fragment peak was calculated and exported to Excel for comparison across groups.

2.6. Assessment of inflammatory mediators

Cell culture supernatants, collected at 3 and 24h, were centrifuged at $10,000 \times g$ for 5min, aliquoted, and frozen at −80 °C until use. Luminex Multiplex-immunoassay for simultaneous analysis of inflammatory cytokines, tumor necrosis factor (TNF)-α, interleukin (IL)-8, IL-1β, IL-1RA, IL-6, and IL-10 using HCYTOMAG-60K Milliplex MAP Human cytokine magnetic bead panel was performed. The ratio of IL-1β to IL-1RA was calculated. Transforming growth factor (TGF)-β1 production was determined using TGF-β1 assay kit (Quantikine ELISA, Human TGF-β1 Immunoassay; R&D, USA), while the nitric oxide (NO) release was assessed with Griess reagent system (Promega, Madison, WI, USA).

2.7. Statistical analysis

Statistical analyses were performed with IBM SPSS Statistics for Windows (Version 22.0. Armonk, NY: IBM Corp). Unpaired Student's t-test was used for comparisons of two samples (cells characterization in the presence of CSnp experiments and for relative abundance of proteins in comparison to control group). One-way analysis of variance and Tukey's post-hoc tests were applied to compare multiple samples (differential expression of selected proteins across experimental groups and analysis of inflammatory mediators). P-value <0.05 was considered statistically significant.

3. Results

3.1. Cells characterization in the presence of CSnp

MTT assay demonstrated that CSnp did not affect MQ and PdLF cell viability for up to 72h (Fig. 1A,D). Higher MQ spreading area was observed in the presence of CSnp at 48 and 72h ($P < 0.05$) (Fig. 1B and C). PdLF spreading increased over time without significant difference (Fig. 1E and F). Analysis of phalloidin-TRITC stained PdLF images demonstrated higher expression of actin filaments in the presence of CSnp than unstimulated cells ($P < 0.01$) (Fig. 1G and H). The number of migrating PdLF in coculture with MQ was presented after subtracting
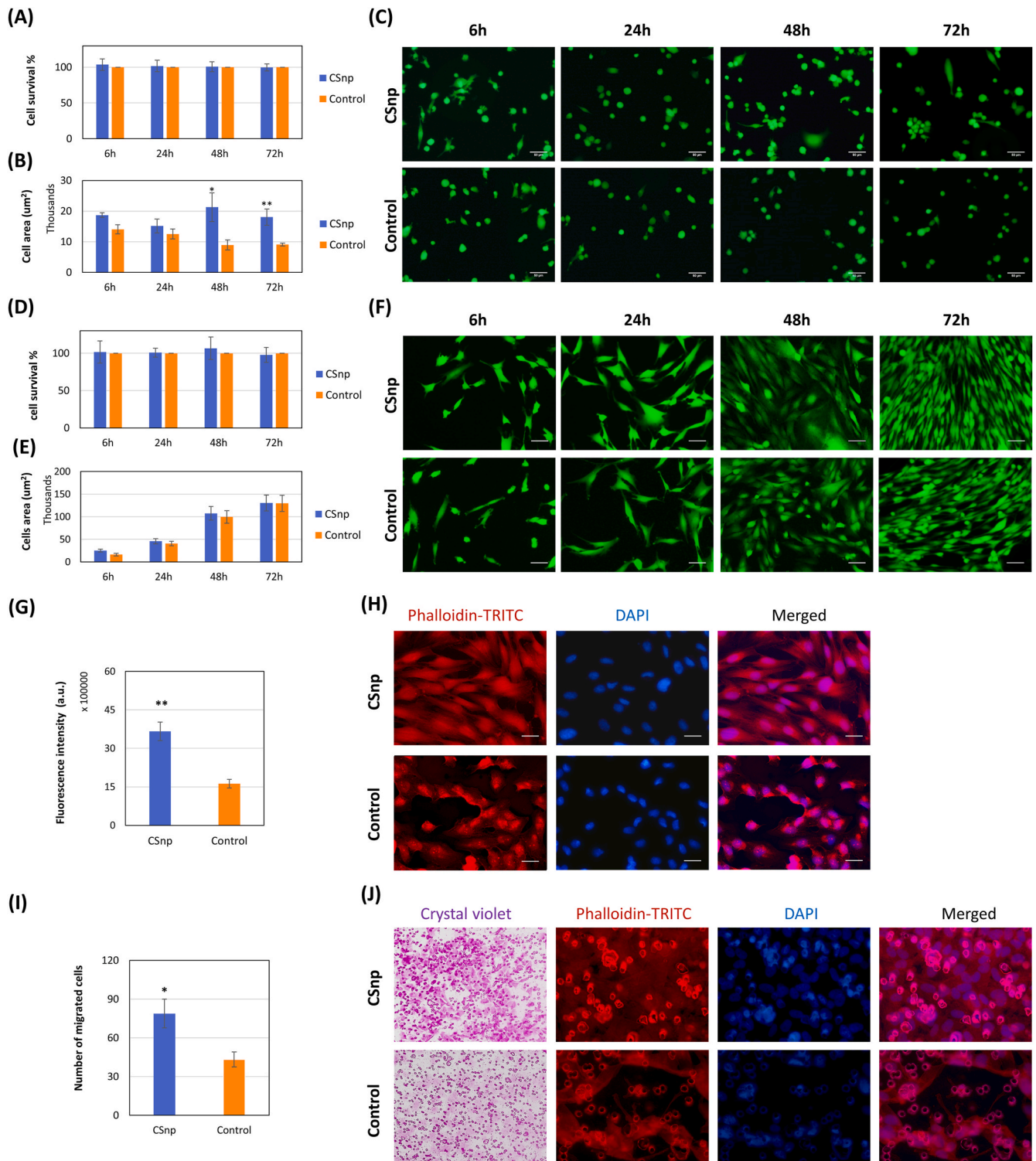

Fig. 1. Characterization of cells in the presence of CSnp. MTT viability assay of MQ (A) and PdLF (D). Cells spreading area of MQ (B) and PdLF (E). Calcein AM-stained images (20x magnification, scale bar = 50 μm) at 6, 24, 48 and 72h of MQ (C) and PdLF (F). F-actin cytoskeleton characterization of PdLF at 72h (G) and images of PdLF stained with phalloidin-TRITC and nuclei counterstained with DAPI (40x magnification, scale bar = 25 μm) (H). (I) Transwell migration assay of PdLF at 24h. (J) Migrated PdLF; crystal violet-stained and phalloidin-TRITC/DAPI images. * represents statistically significant difference (n = 3), $p < 0.05$. **, $p < 0.01$.

the PdLF that migrated in the monoculture setup. CSnp resulted in significantly more migrating PdLF (~2-fold higher) compared to control ($P < 0.05$) (Fig. 1I and J).

3.2. Intracellular uptake and trafficking of CSnp

Dark contrast rounded shapes indicative of CSnp were observed in the TEM images of MQ and PdLF. Cells appeared to incorporate CSnp to the plasma membrane invaginations or protrusions of distinct ultrastructure. At 3h, small clathrin-coated pits on the cell membrane were observed, suggestive of clathrin-mediated endocytosis (Fig. 2A–C,H,I). Plasma membrane protrusion characteristic of macropinocytosis was observed (Fig. 2G). Intracellularly, CSnp were detected within endosomes closer to cell membrane (Fig. 2C–E,H-J). At 24h, CSnp were frequently observed in association with membrane ruffles indicating their uptake via macropinocytosis or phagocytosis in case of aggregated nanoparticles (Fig. 3B,C,I-K). After internalization, most of CSnp were contained in membrane-bound organelles (endosomes, multivesicular bodies, and lysosomes), few CSnp were located freely inside the cytosol, and none were found to be trafficked into the nucleus. Some signs of degrading CSnp were observed within MQ lysosomes (Fig. 3G).

3.3. Global protein expression profiles of differentiated macrophages

A total number of 2061 and 1832 proteins were identified in the 3 and 24h sets respectively. After filtering the LC-MS/MS proteomics data 1733 and 1027 proteins were quantified with 2 or more unique peptides in 3 and 24h data respectively. The distribution of these proteins among different groups is presented (Fig. 4A). In functional categorization, according to the "biological process", most of the proteins belong to the categories of cellular process, and metabolic process (Fig. 4B). Under the "molecular function", most of the proteins belong to the categories of

protein binding, and catalytic activity, followed by structural molecule activity (Fig. 4C). Based on the "cellular component", most proteins were in cells and organelles followed by protein-containing complexes. There were no significant changes among the groups according to GO classification (Fig. 4D).

The heat maps depicted the changes in protein expression among groups, and the hierarchical clustering clearly separated the control group from experimental groups at 3h, whereas, biofilm group was separated from other groups at 24h, followed by separation of control group from CSnp-treated biofilm and CSnp groups, highlighting the changes that occurred in the global protein profiles relative to the control over time (Fig. 4E). In PCA, performed to describe the variation in the data sets, CSnp-treated biofilm and CSnp groups appeared to be in a matching position with the control along component one, which carries most of the variance (84.46%) at 24h. This observation corroborates with groups' hierarchical clustering (Fig. 4F).

Volcano plots demonstrated the protein abundance in each experimental group relative to control at 24h (Fig. 5A, Fig. 6A,F). STRING analysis of the protein interaction networks of the biofilm DEP (Fig. 5B and C) revealed functional enrichments of multiple biologic processes (Fig. 5D and E), while according to the Kyoto Encyclopedia of Genes and Genomes (KEGG) pathway analysis, biofilm upregulated proteins showed functional enrichment of cholesterol metabolism, necroptosis, and lysosomes (Fig. 5E). Upregulated proteins in CSnp-treated biofilm were involved in metal sequestration by antimicrobial proteins while downregulated proteins were related to ferroptosis and hypoxia-inducible factor signaling pathway (Fig. 6B–E). DEP of CSnp did not show significant functional pathway enrichments (Fig. 6F).

Comparing relative abundance of proteins between treated and untreated biofilm at 3h showed that CSnp-treated biofilm downregulated *MIF, CYB5R1,* and *SERPINB1*, but showed higher expression of *IKBKG* (Fig. 7A–C). At 24h, more proteins were significantly differentiated
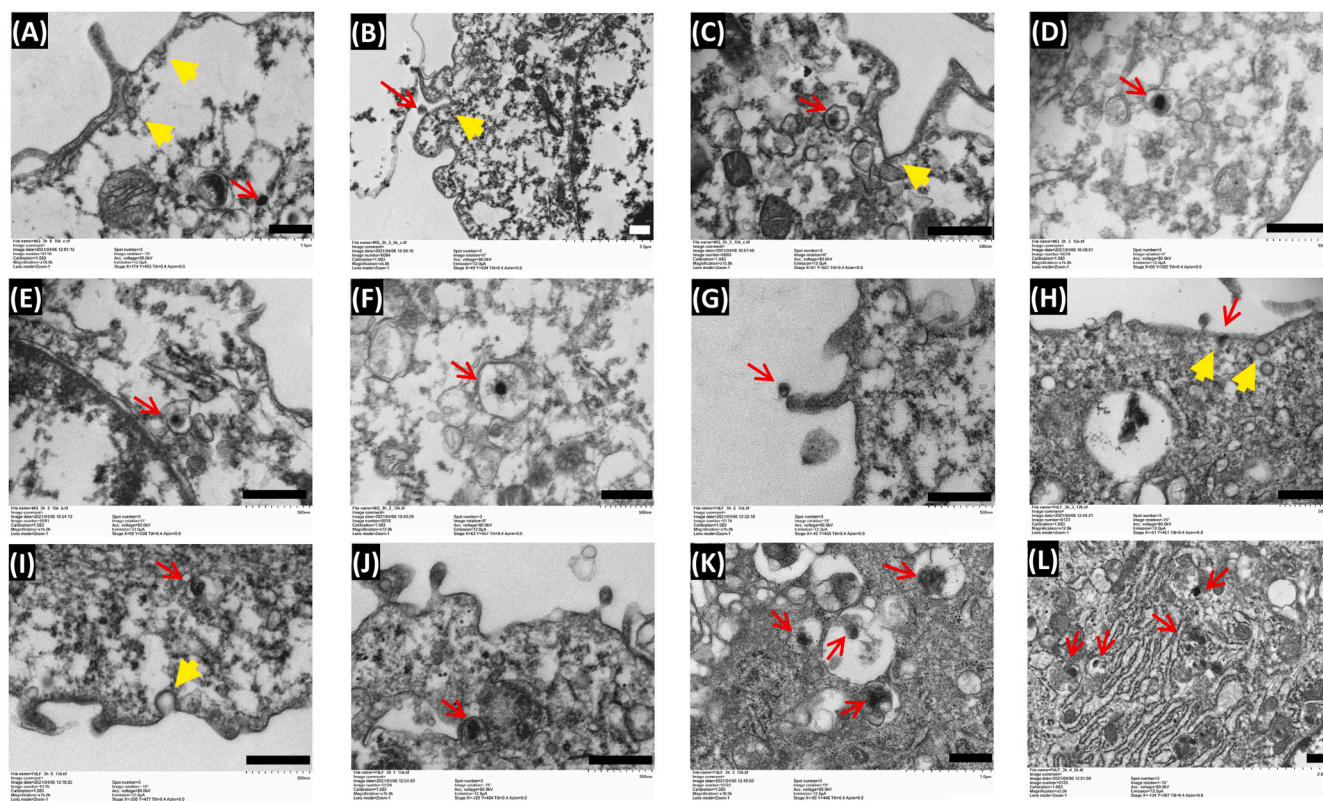

Fig. 2. TEM images of MQ (A–F) and PdLF (G–L) at 3h showing internalization and intracellular trafficking of CSnp. Internalized CSnp were observed in membrane-bound organelles; endosomes, lysosomes, and multivesicular bodies. Open red arrows point to CSnp, yellow closed arrows indicate invaginations of clathrin-coated pits, scale bar = 500 nm.
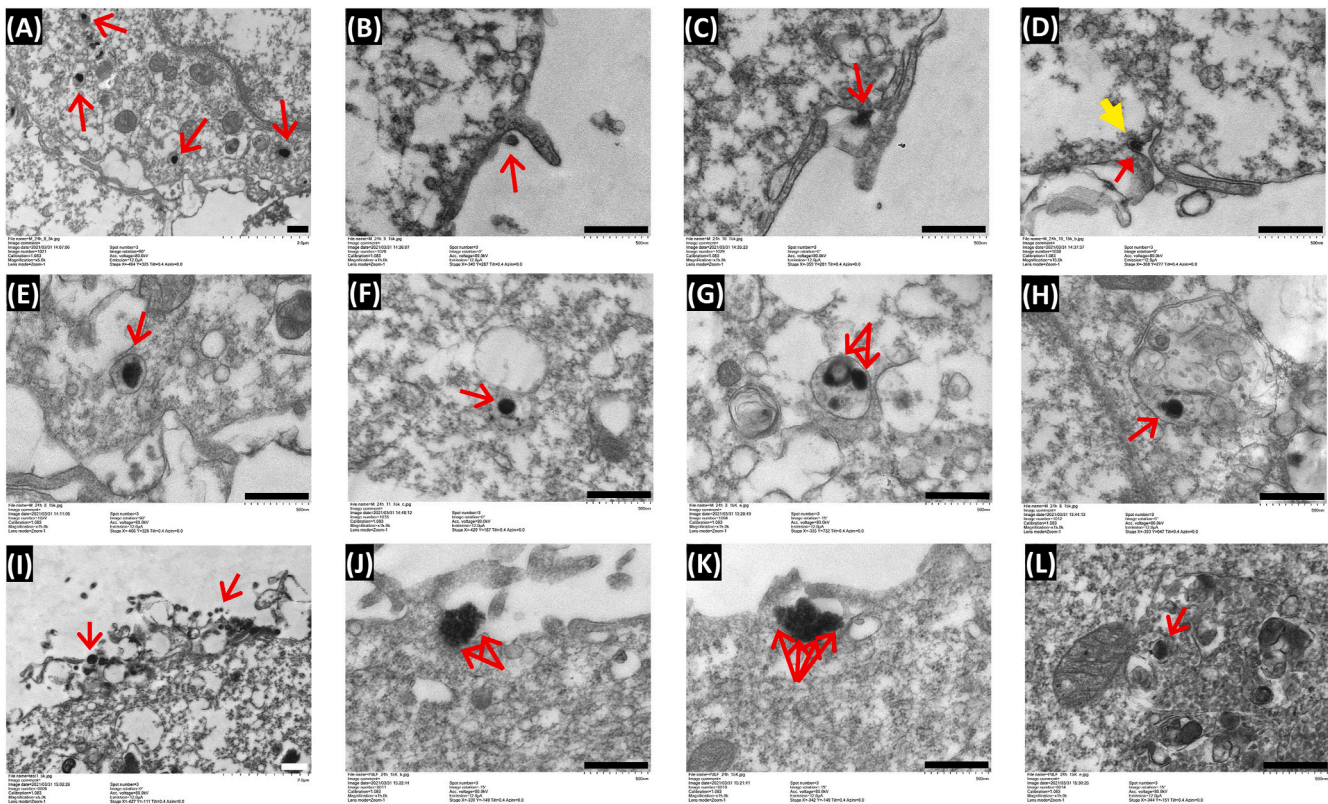
Fig. 3. Transmission electron micrographs of MQ (A–H) and PdLF (I–L) at 24h showing internalization and intracellular trafficking of CSnp. CSnp were observed in association with plasma membrane protrusions indicating macropinocytosis and phagocytosis (B,C,I–K). Internalized CSnp were observed in membrane-bound organelles; endosomes, lysosomes, and multivesicular bodies. Signs of degrading CSnp were seen in MQ lysosomes (G). Open red arrows point to CSnp, yellow closed arrows indicate invaginations of clathrin-coated pits, scale bar = 500 nm.

between CSnp-treated biofilm and untreated biofilm compared to 3h. CSnp-treated biofilm resulted in downregulation of *LAMP1, PTGS1, C1QBP,* and *CTSG* compared to biofilm, while upregulated *SOD1, SOD2, NAMPT, SERPINB1, PRDX1, PRDX5, PTMA,* and *TXN* (Fig. 7D–F).

3.4. Validation of candidate proteins

PRM assay confirmed that biofilm downregulated *SOD1, SOD2, NAMPT, PRDX1,* and *SERPINB1* (Table 1). Contrarily, CSnp treatment of the biofilm rescued the expression of *SOD1, SOD2,* and *NAMPT* to levels comparable to the control. *SERPINB1* was significantly upregulated by CSnp (1.7-folds) followed by CSnp-treated biofilm (1.3-folds), while biofilm resulted in its downregulation (0.6-fold).

3.5. Assessment of inflammatory mediators

CSnp treatment resulted in decreased expression of IL-1β and NO compared to biofilm ($P < 0.05$). Contrarily, CSnp treatment enhanced the production of IL-10 and TGF-β1 ($P < 0.01$, 24h). IL-6 level increased over time, and CSnp-treated biofilm resulted in the highest level at 24h ($P < 0.05$) (Fig. 8).

4. Discussion

Engineering nanosized immunomodulatory bioactive materials provide several strategies for the modulation of immune system in tissue regeneration and wound healing [31]. Herein, we elucidated the immunomodulatory effects exerted by engineered bioactive CSnp applied as an antibiofilm treatment on MQ and their interaction with PdLF. Additionally, the proteomic and cytokine profiles were evaluated upon stimulating the cells with CSnp alone in the absence of biofilm

challenge to reveal the immunomodulatory effect of CSnp per se. CSnp were internalized via clathrin-mediated endocytosis, macropinocytosis, and phagocytosis subsequent to electrostatic interaction of cationic CSnp with negatively charged plasma membrane in accordance with previous investigations [32,33]. Initially, at 3h, clathrin pits were seen and internalized CSnp were located closer to cell membrane in membrane-bound vesicles. Observation of membrane protrusions characteristic of macropinocytosis and phagocytosis more frequently at 24h indicate uptake of relatively larger particles that might have swollen/-aggregated. CSnp augmented MQ cell spreading indicative of increased cell surface area which has been suggested to aid in particle binding and phagocytosis [34]. Visualizing cellular uptake of CSnp was necessary prior to conducting MQ proteomic analysis to ensure that observed changes in protein expression were associated with direct effect of CSnp intracellularly.

MQ were cocultured with PdLF to contemplate the vital role of paracrine signaling that influences the outcome of inflammatory/healing processes in AP [35]. Primary endodontic infections are commonly polymicrobial in nature, contrarily one or few bacterial species are involved with secondary infections [36,37]. *E. faecalis* were employed in this study because of their strong biofilm-forming properties, ability to survive harsh environmental conditions, such as post-treatment endodontic environment, while being associated with post-treatment apical periodontitis [38,39]. Although using mono-species biofilm represents a limitation, it allowed for mechanistic investigation and understanding of MQ signaling pathway in a standard manner which was specifically crucial for the proteomics assays. Since understanding the mechanism of *E. faecalis* biofilm-induced inflammatory signaling could aid in developing treatments for persistent AP, our proteomics data set has also been analyzed to reveal modifications in MQ challenged with *E. faecalis* biofilm.
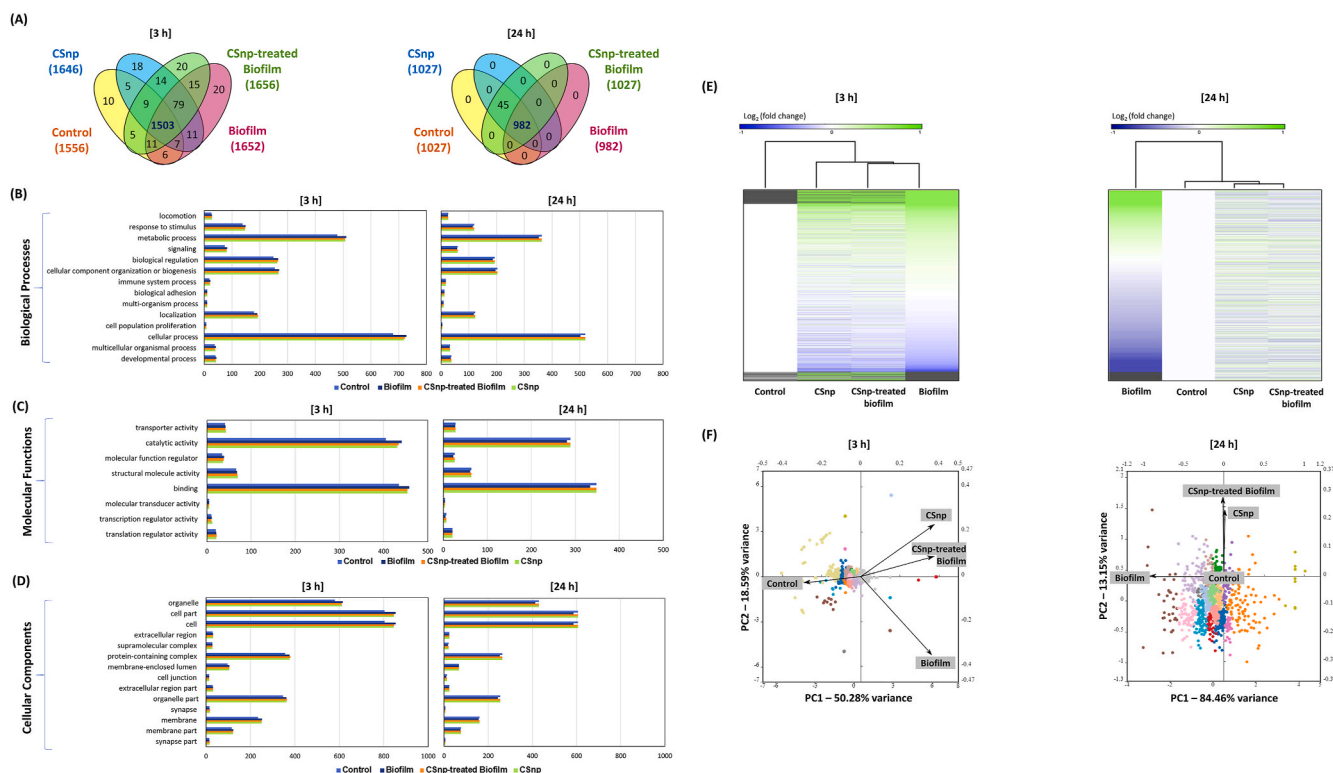
Fig. 4. Global analysis of TMT-MS proteomics data. Identified proteins with 2 or more unique peptides and quantified in all biological replicates of at least one group were included. (A) Venn diagrams showing the distribution of quantified proteins among groups at each time point, 3h, and 24h. Quantified proteins were categorized using Panther Classification on Gene Ontology, based on their "biological process" (B), "molecular function" (C), and "cellular component" (D). (E) Heat maps presentation of hierarchical clustering of the proteins showed separation of control from the experimental groups at 3h, whereas, at 24h, the biofilm group was separated from the other groups, followed by separation of control from CSnp and CSnp-treated biofilm. The blue color represents low and the green color represents high expression levels. In case the protein was not detected in a group, the cells were left blank (the black color in the heatmap indicates the missing values). (F) Principal component analysis yielded 3 components, of which the first two are represented in the figure; At 3h, PC1 explained 50.28%, and PC2 – 18.59%, while at 24h PC1 explained 84.46%, and PC2 – 13.15% of the total variance.

Multiplexed proteomics using isobaric tags, particularly TMT which was applied in this study, enables global quantification of proteins relatively across multiple samples [40]. Protein expression analysis is advantageous among large-scale approaches since microarray analysis of mRNA identification does not always correlate with protein expression [41]. Proteomics results denote a snapshot in time and cannot represent dynamic regulation of MQ functions, thereby, to overcome this limitation we employed more than one-time point and used bioinformatic methods (*in-silico* analysis). To validate relative abundance of selected proteins, we used PRM which has been applied as targeted MS approach following discovery-based proteomics [42].

Proteomics data of 3h time point showed that *MIF*, a pro-inflammatory mediator involved in innate immune response to bacterial pathogens was upregulated in biofilm, while CSnp reduced it significantly. Biofilm upregulated *CYB5R1* which is involved in desaturation and elongation of fatty acids, and cholesterol biosynthesis. Lipids are critical metabolites during MQ polarization, M1 synthesize fatty acids to use them as precursors for synthesis of inflammatory mediators [43]. Whereas CSnp-treated biofilm increased *IKBKG*, a regulatory subunit of IKK core complex which phosphorylates inhibitors of NF-kappa-B (NF-κB) that orchestrates immunological responses. At 24h, multiple proteins involved in the metabolic pathway of tricarboxylic acid cycle, which is intact in anti-inflammatory MQ [44], were downregulated (*COX5B, ATP5H, CYCS, MDH2, and LDHB*) or not identified (*COX6C, ATP5D, SDHA, IDH3A, and UQCR10*) in biofilm group, but they were expressed in both CSnp groups at levels comparable to control (Supplementary Table 1).

On the other hand, upregulated proteins in biofilm group at 24h included lysosome-associated membrane protein 1 (*LAMP1*) which is

required for phagosome maturation. Phagosomes containing pathogens like *Salmonella* recruit *LAMP1* from Golgi-derived vesicles without fusing with lysosomes [45]. It was suggested that other intracellular pathogens might use similar strategies to maintain structural integrity of phagosomal membrane, thus providing an appropriate niche for their replication [45]. Biofilm upregulated prostaglandin G/H synthase 1 (*PTGS1*), known as cyclo-oxygenase 1, which plays a central role in the inflammatory cascade by converting arachidonic acid to prostaglandin H2, which in turn is converted to bioactive prostanoids. Cyclo-oxygenases (COX-1, COX-2) are involved in inflammation and pain signaling pathways in periapical tissues [46]. Additionally, biofilm significantly increased complement C1q binding protein (*C1QBP*), which acts as C1q receptor and is involved in inflammation and infection processes. C1q, an important recognition molecule of innate immune response, triggers inflammation via activation of classical complement pathway to clear pathogens and plays important role in modulating MQ activation [47].

Leukocyte elastase inhibitor (*SERPINB1*) which protects the cell from proteases released during stress or infection has been reported as potential regulator of the inflammatory response in AP [48]. It also influences cell migration suggesting its role in wound healing process [49]. *SERPINB1*-depleted THP1 cells have been shown to cause elevated IL-1β secretion and pyroptosis, signifying its role in minimizing host damage from detrimental inflammation [50]. In our study, *SERPINB1* was increased initially in biofilm, while at 24h it was upregulated in both CSnp-treated biofilm and CSnp, but not detected in biofilm group. PRM results successfully confirmed *SERPINB1* upregulation by CSnp at 24h. *SERPINB1* regulates inflammatory responses through its inhibitory effect on serine proteases, known to degrade extracellular matrix in AP,
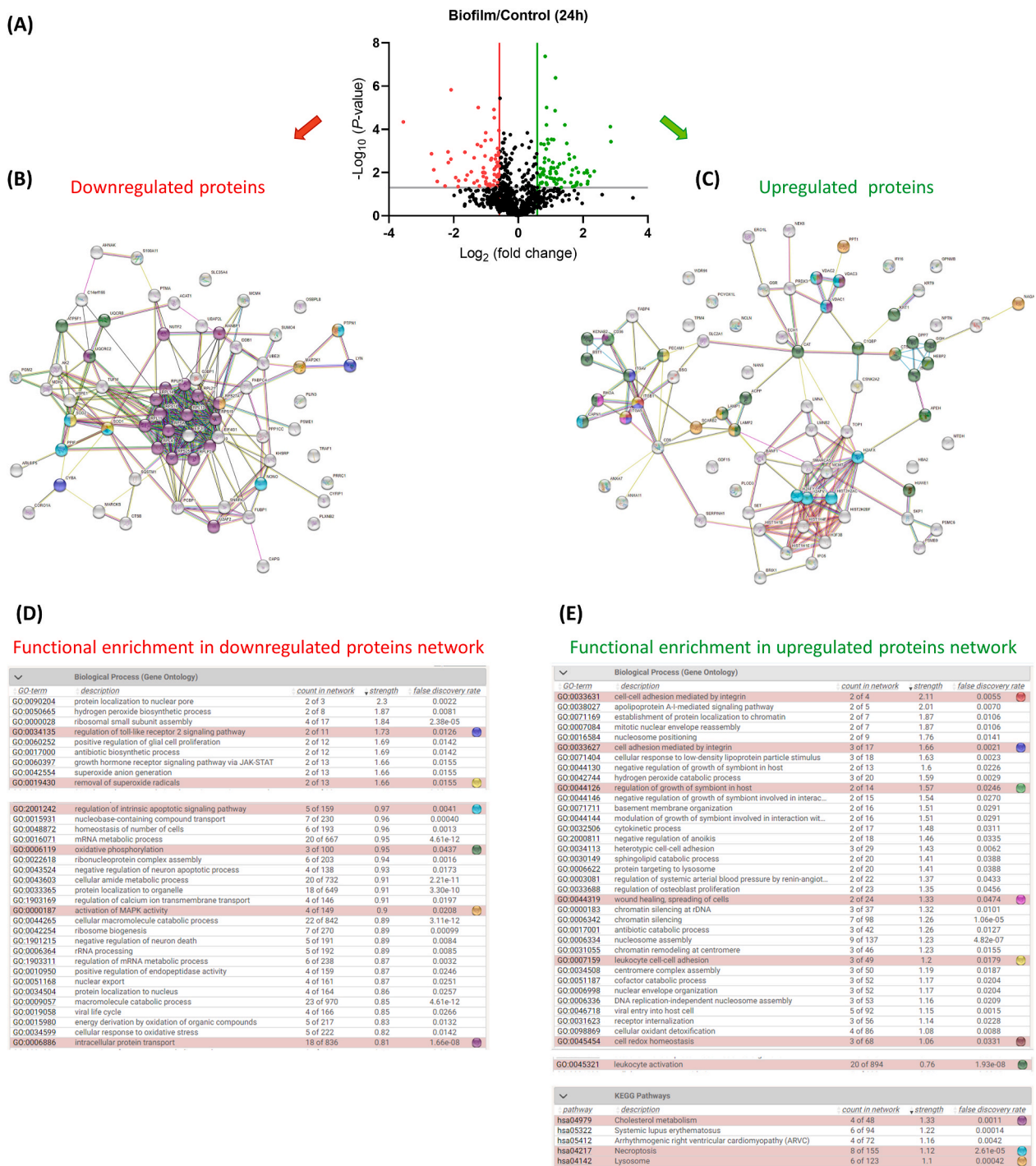
(A)

Biofilm/Control (24h)

(B) Downregulated proteins

(C) Upregulated proteins

(D)

Functional enrichment in downregulated proteins network

(E)

Functional enrichment in upregulated proteins network

Fig. 5. Proteome profiling of the macrophage inflammatory response to biofilm at 24 h. (A) Volcano plot of biofilm versus the control group. STRING protein-protein interaction networks of the DEP; 66 out of the 68 downregulated proteins participated in the network (B), and 76 out of the 78 upregulated proteins (C). Functional enrichments in the protein networks of biofilm group; (D) Downregulated proteins showed enrichment in biological processes, such as regulation of TLR2 signaling and intracellular protein transport. (E) Upregulated proteins were involved in biological processes such as cellular adhesion, regulation of growth of symbiont in host, and leukocyte activation. Whereas, in KEGG pathways, cholesterol metabolism, necroptosis, and lysosome showed enrichment. In the volcano plot, the vertical green line represents 1.5-fold upregulation (Log_2 fold change = 0.585), and the vertical red line represents 1.5-fold downregulation (Log_2 fold change = −0.585). Green and red dots correspond to proteins that are significantly up-and-down-regulated, respectively, with a cutoff value of ≥1.5-fold change and a P value of 0.05 (horizontal grey line at -log_{10} P-value = 1.301). The STRING networks nodes represent proteins, and nodes color represent the proteins involved in the functional enrichments in each network. Edges represent protein-protein associations. Connecting lines represent interactions with at least medium confidence score (0.400). False discovery rate, describes how significant the enrichment is ($P < 0.05$).
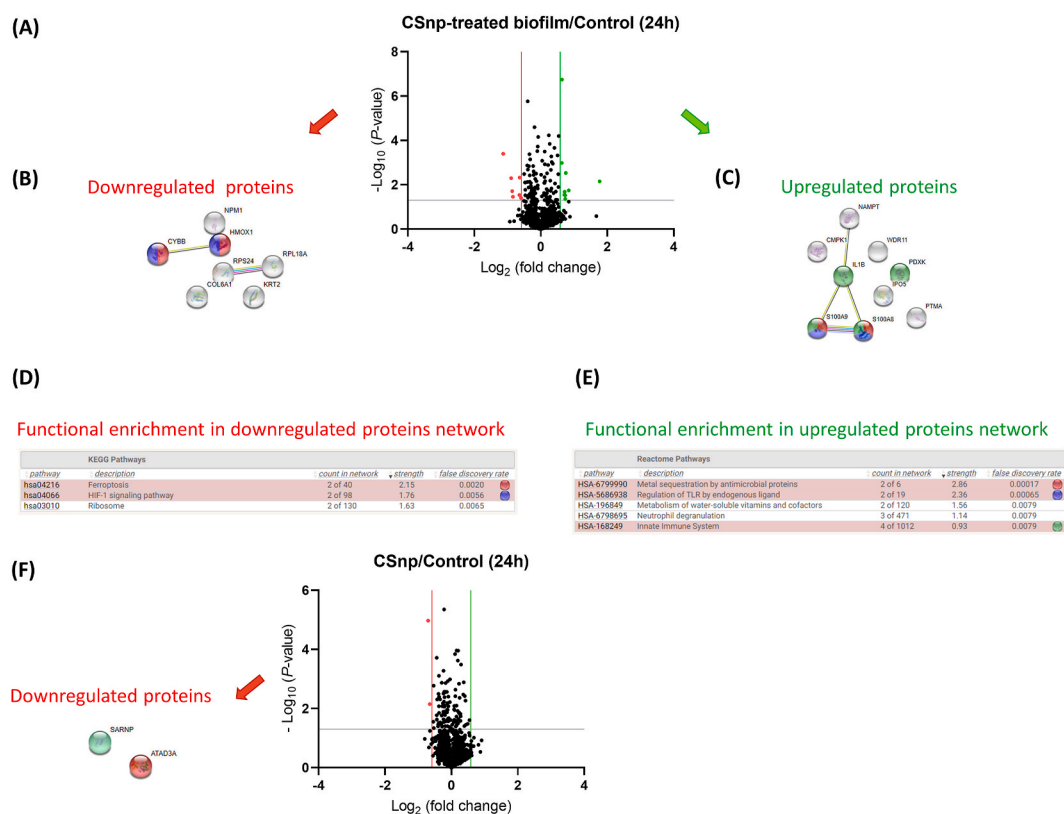
Fig. 6. Proteome profiling of the macrophage inflammatory response to CSnp-treated biofilm and CSnp at 24 h. (A) Volcano plot of CSnp-treated biofilm versus the control group. STRING protein-protein interaction networks of the DEP, the 7 downregulated proteins participated in the network (B) and the 9 upregulated proteins in the other depicted protein network (C). CSnp-treated biofilm group downregulated proteins (D) showed enrichment in KEGG pathways related to ferroptosis, while upregulated proteins (E) were related to metal sequestration by antimicrobial proteins and regulation of TLR by endogenous ligand in Reactome pathways. (F) Volcano plot of CSnp versus the control group. The 2 downregulated proteins were not involved in functional enrichment pathways in the STRING tool.

such as cathepsin-G (*CTSG*) [51], which was >1.5-folds increased in biofilm. Additionally, upregulation of *SERPINB1* could explain in part preservation of cells viability after interaction with CSnp.

Upregulated proteins in CSnp-treated biofilm at 24h showed functional enrichment in metal sequestration by antimicrobial proteins. Another way by which CSnp could defy bacterial infection is via downregulating proteins involved in ferroptosis pathway, an iron-dependent and ROS-reliant cell death resulting from loss of plasma membrane selective permeability due to intense membrane lipid per-oxidation and oxidative stress. Ferroptosis denotes favorable conditions for bacterial infection since bacteria require iron to proliferate [52]. Reactive species derived from oxygen and nitrogen, such as, superoxide (O_2^-), hydroxyl anion ($^{\bullet}OH$), and nitric oxide ($NO^{\bullet}$), play important role in disease progression, whereas antioxidants antagonize their effects to maintain hemostasis. In comparison to untreated biofilm, CSnp upregulated proteins with antioxidant activities (*SOD1, SOD2, PRDX1, PRDX5,* and *TXN*) which would aid in destroying toxic radicals that are produced within the cells. They ensure critical monitoring of cellular ROS levels and conserve normal redox homeostasis essential for cell viability (graphical abstract schematic). *SOD1,* which catalyzes super-oxide dismutation, was associated with H_2O_2 production and also contributed to M2 alternative activation that was regulated by redox-dependent STAT6 translocation [53]. *PRDX1* and *PRDX5* exert protective effects on cellular toxicity against increased cellular H_2O_2 levels induced by oxidative and inflammatory stresses [54]. Following oxidation of *PRDX*, they form disulfide linkages, while they return to their active form after reduction by *TXN* [55]. Overproduction of H_2O_2 causes tissue injury through DNA and protein damage, and could also act as intracellular second messengers, activating a variety of signal trans-duction pathways such as MAPK and RANK/RANKL pathways [56]. An

altered balance between highly ROS production by phagocytic cells in periapical lesions and its elimination was suggested to contribute to periapical damage and bone loss in chronic AP [57].

CSnp upregulated proteins possessing immunoregulatory effects, such as Nicotinamide phosphoribosyltransferase (*NAMPT*) and prothy-mosin alpha (*PTMA*). *NAMPT* is the rate-limiting component in mammalian nicotinamide adenine dinucleotide biosynthesis. When secreted extracellularly, it acts both as a cytokine with immunomodu-lating properties and an adipokine with anti-diabetic properties [58,59]. *PTMA* promotes cell proliferation, modulates inflammatory response via acting as TLR agonist, and generates the appropriate cytokine milieu enhancing the activation of effector cells [60]. The proteins upregulated in MQ interacting with CSnp alone with >1.5-fold increase but not statistically significant compared to control (Supplementary Fig. 1) showed significant functional enrichment in the protein-protein inter-action networks related to multiple biological processes with regulatory functions such as regulation of non-canonical NF-κB signaling, protein and cytokine secretion, and cell motility and migration. This observation is worth mentioning since it demonstrates the regulatory effect of CSnp on MQ even in the absence of microbial challenge.

We further investigated the multiplex cytokine profile of cell culture supernatants. The balance between pro-and anti-inflammatory signals is crucial during inflammatory and healing processes in AP [61]. Herein, *E. faecalis* biofilm resulted in significantly higher levels of IL-1β and NO, in accordance with previous studies which reported excessive secretion of IL-1β and MQ death stimulated by *E. faecalis* [62,63]. CSnp treatment suppressed pro-inflammatory mediators; NO and IL-1β. Conversely, CSnp-treated biofilm resulted in significantly higher anti-inflammatory mediators (IL-10 and TGF-β1) which antagonize proinflammatory re-sponses and possess pro-wound healing properties [64]. The relatively
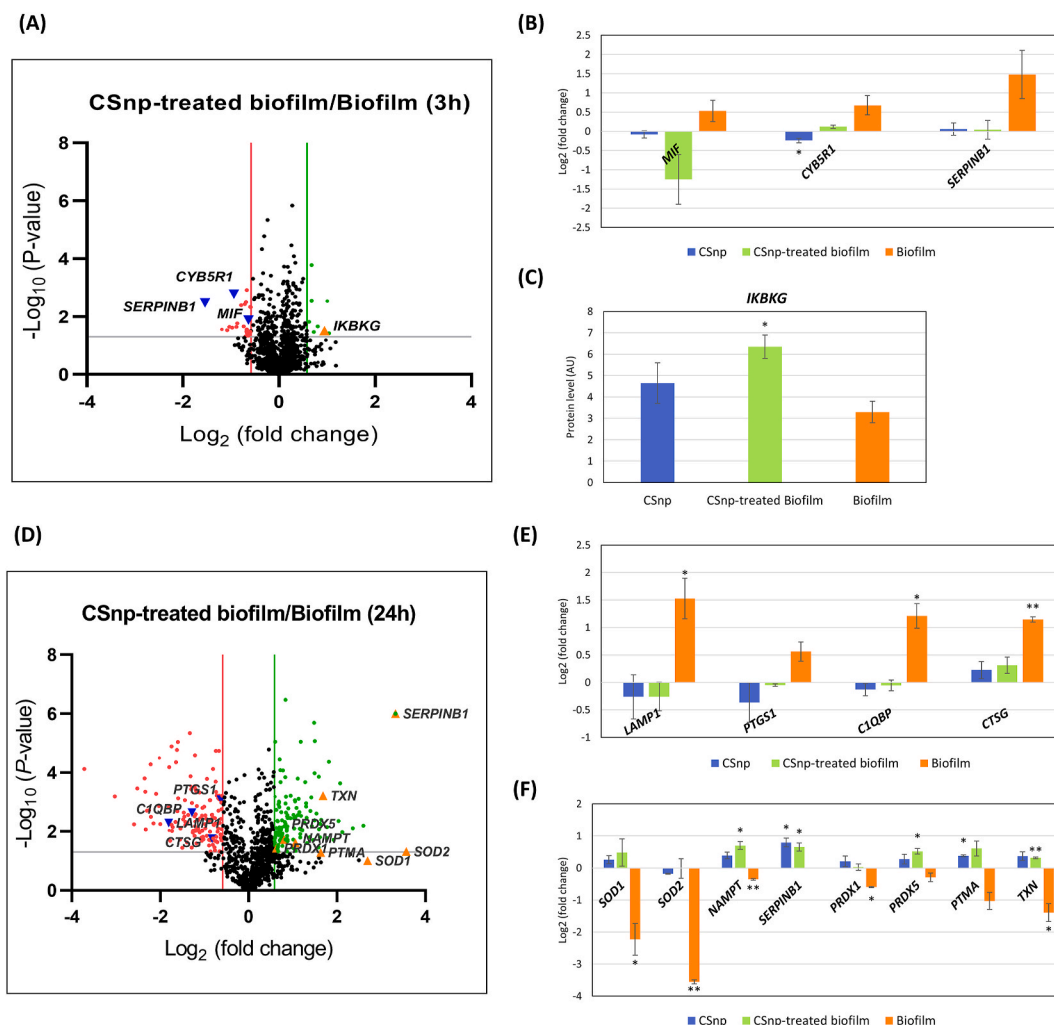
Fig. 7. Differentially abundant proteins of CSnp-treated biofilm versus biofilm group. (A) Volcano plot showing abundance of all proteins in CSnp-treated biofilm relative to biofilm group at 3h. The names of selected differentially expressed proteins are labeled. (B) Bar graphs showing $\log_2$ fold change of the selected proteins across the experimental groups relative to negative control at 3h. (C) Bar graph showing *IKBKG* protein levels among experimental groups as it was not detected in the negative control at 3h. (D) Volcano plot showing abundance of all proteins in CSnp-treated biofilm relative to biofilm group at 24h. Bar graphs showing $\log_2$ fold change of the selected proteins across the experimental groups relative to negative control at 24h, upregulated (E), and downregulated (F) in biofilm. Data represent mean $\pm$ SEM, (n = 2), *$P < 0.05$.

Table 1
Relative abundance of selected proteins validated using PRM-targeted proteomics.

Accession ID	Protein name	Gene name	LOG2 Fold Change			
			Biofilm/Control	CSnp-treated biofilm/Control	CSnp/Control	CSnp-treated biofilm/Biofilm
P00441	Superoxide dismutase [Cu–Zn]	*SOD1*	−2.314 ↓ (1.681)	−0.286 (0.561)	0.483 (0.315)	1.213 ↑ (0.561)
P04179	Superoxide dismutase [Mn]	*SOD2*	−2.343 ↓ (1.557)	−0.523 (0.416)	−0.003 (0.103)	1.105 ↑ (0.416)
Q06830	Peroxiredoxin-1	*PRDX1*	−2.084 ↓ (1.259)	−0.676 ↓ (0.289)	−0.204 (0.345)	0.592 ↑ (0.614)
P43490	Nicotinamide phosphoribosyl-transferase	*NAMPT*	−1.657 ↓ (1.117)	0.067 (0.116)	0.191 (0.260)	1.329 * ↑ (0.116)
P30740	Leukocyte elastase inhibitor	*SERPINB1*	−1.566 ↓ (1.610)	0.394 (0.316)	0.783 * ↑ (0.007)	1.203 ↑ (0.316)

Data represented as LOG2 fold change and (standard error of the mean). ↓ indicates >1.5-fold downregulated and ↑ indicates >1.5-fold upregulated. * indicates statistical significance ($P < 0.05$).

higher expression of IL-8 in CSnp at 24h might explicate the higher migration of PdLF since it chemoattracts fibroblasts and accelerates their migration [65]. IL-6, which was increased in CSnp-treated biofilm but not in CSnp alone, plays a significant role in the kinetics of pulpal and periapical inflammatory reactions to bacterial infection and affects immune cells maturation and differentiation [66]. It possesses both pro-and anti-inflammatory properties, where its final effect depends on the effector cells and interplay with other cytokines [57]. IL-6 has been
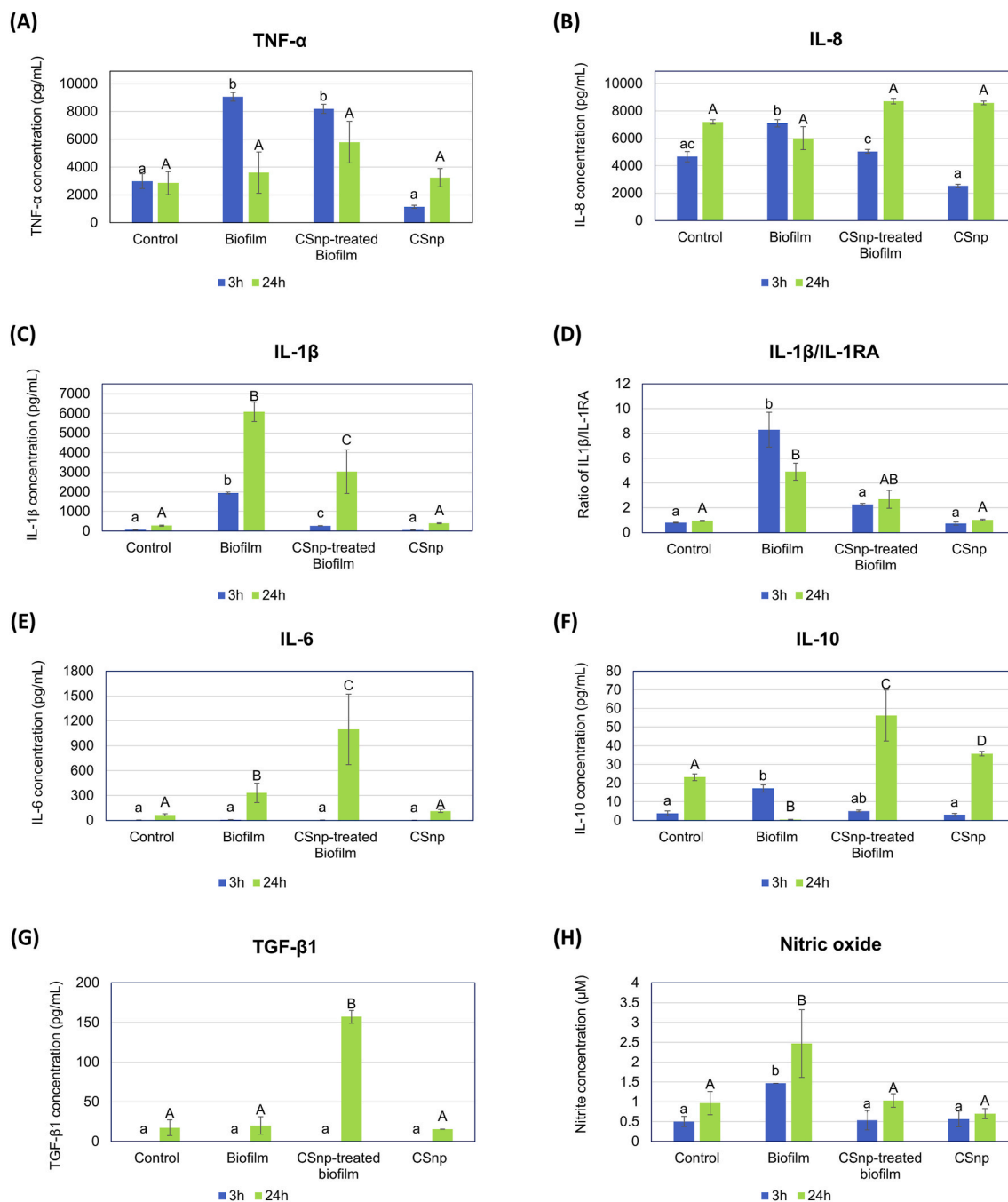
Fig. 8. Expression of inflammatory mediators. (A) TNF-α, (B) IL-8, (C) IL-1β, (D) Ratio of IL-1β/IL-1RA, (E) IL-6, (F) IL-10, (G) TGF-β1, and (H) Nitric oxide. Data represent mean ± SD, (n = 4). Different lowercase letters represent significant differences between groups at 3h, $P < 0.05$. Different uppercase letters represent significant differences between groups at 24h, $P < 0.05$.

shown to modulate TGF-β1 expression to regulate wound healing [67]. Higher IL-6 secretion in CSnp-treated biofilm might have also mediated the increased IL-10 production since it has been shown to help MQ polarization into M2 phenotype [68].

5. Conclusions

In conclusion, engineered bioactive CSnp were internalized via macropinocytosis, clathrin-mediated endocytosis, and phagocytosis. CSnp were trafficked intracellularly within membrane-bound organelles, endosomes, multivesicular bodies, and lysosomes. CSnp maintained cells viability up to 72h while promoted MQ spreading and PdLF migration. CSnp modified the proteomic and cytokine profiles of MQ in

a way that modulated biofilm-mediated inflammation. Proteomics elucidated that CSnp upregulated proteins involved in immunoregulatory functions and antioxidant activities, while downregulated proteins were related to ferroptosis pathway that contributes to bacterial nourishment. CSnp promoted production of anti-inflammatory/pro-regenerative mediators but suppressed pro-inflammatory ones. Hence, CSnp could rescue persistent post-treatment inflammation. Further *in-vivo* studies of CSnp immunomodulatory effects are warranted to confirm its potential to promote periapical tissue healing.

CRediT authorship contribution statement

Hebatullah Hussein: Conceptualization, Methodology, Formal analysis, Investigation, Data curation, Writing – original draft, Visualization, Writing – review & editing. **Anil Kishen:** Conceptualization, Methodology, Resources, Funding acquisition, Project administration, Supervision, Writing – review & editing.

Declaration of competing interest

The authors declare that they have no known competing financial interests or personal relationships that could have appeared to influence the work reported in this paper.

Acknowledgments

Appendix A. Supplementary data

Supplementary data to this article can be found online at https://doi.org/10.1016/j.bioactmat.2021.09.032.

References

[1] Y. Qie, H. Yuan, C.A. von Roemeling, Y. Chen, X. Liu, K.D. Shih, J.A. Knight, H. W. Tun, R.E. Wharen, W. Jiang, B.Y. Kim, Surface modification of nanoparticles enables selective evasion of phagocytic clearance by distinct macrophage phenotypes, Sci. Rep. 6 (2016), 26269, https://doi.org/10.1038/srep26269.

[2] P.N. Nair, On the causes of persistent apical periodontitis: a review, Int. Endod. J. 39 (2006) 249–281, https://doi.org/10.1111/j.1365-2591.2006.01099.x.

[3] I.J. Márton, C. Kiss, Protective and destructive immune reactions in apical periodontitis, Oral Microbiol. Immunol. 15 (2000) 139–150, https://www.ncbi.nlm.nih.gov/pubmed/11154396.

[4] C.S. Tibúrcio-Machado, C. Michelon, F.B. Zanatta, M.S. Gomes, J.A. Marin, C. A. Bier, In, The global prevalence of apical periodontitis: a systematic review and meta-analysis, t. Endod. J. 54 (2021) 712–735, https://doi.org/10.1111/iej.13467.

[5] J.J. Segura-Egea, J. Martín-González, L. Castellanos-Cosano, Endodontic medicine: connections between apical periodontitis and systemic diseases, Int. Endod. J. 48 (2015) 933–951, https://doi.org/10.1111/iej.12507.

[6] B. Karabucak, A. Bunes, C. Chehoud, M.R. Kohli, F. Setzer, Prevalence of apical periodontitis in endodontically treated premolars and molars with untreated canal: a cone-beam computed tomography study, J. Endod. 42 (2016) 538–541, https://doi.org/10.1016/j.joen.2015.12.026.

[7] Y. Niu, Z. Wang, Y. Shi, L. Dong, C. Wang, Modulating macrophage activities to promote endogenous bone regeneration: biological mechanisms and engineering approaches, Bioact. Mater. 6 (2021) 244–261, https://doi.org/10.1016/j.bioactmat.2020.08.012.

[8] Z. Julier, A.J. Park, P.S. Briquez, M.M. Martino, Promoting tissue regeneration by modulating the immune system, Acta Biomater. 53 (2017) 13–28, https://doi.org/10.1016/j.actbio.2017.01.056.

[9] Y. Liang, X. Luan, X. Liu, Recent advances in periodontal regeneration: a biomaterial perspective, Bioact. Mater. 5 (2020) 297–308, https://doi.org/10.1016/j.bioactmat.2020.02.012.

[10] M.M. Islam, M. Shahruzzaman, S. Biswas, M. Nurus Sakib, T.U. Rashid, Chitosan based bioactive materials in tissue engineering applications-A review, Bioact. Mater. 5 (2020) 164–183, https://doi.org/10.1016/j.bioactmat.2020.01.012.

[11] E.I. Rabea, M.E. Badawy, C.V. Stevens, G. Smagghe, W. Steurbaut, Chitosan as antimicrobial agent: applications and mode of action, Biomacromolecules 4 (2003) 1457–1465, https://doi.org/10.1021/bm034130m.

[12] D. Fong, C.D. Hoemann, Chitosan immunomodulatory properties: perspectives on the impact of structural properties and dosage, Future Sci. OA 4 (2018) FSO225, https://doi.org/10.4155/fsoa-2017-0064.

[13] A. Kishen, Z. Shi, A. Shrestha, K.G. Neoh, An investigation on the antibacterial and antibiofilm efficacy of cationic nanoparticulates for root canal disinfection, J. Endod. 34 (2008) 1515–1520, https://doi.org/10.1016/j.joen.2008.08.035.

[14] H. Hussein, A. Kishen, Antibiofilm and immune response of engineered bioactive nanoparticles for endodontic disinfection, J. Clin. Med. 9 (2020), https://doi.org/10.3390/jcm9030730.

[15] H. Hussein, A. Kishen, Engineered chitosan-based nanoparticles modulate macrophage – periodontal ligament fibroblast interactions in biofilm-mediated inflammation, J. Endod. (2021), https://doi.org/10.1016/j.joen.2021.06.017.

[16] B.S. Zolnik, A. González-Fernández, N. Sadrieh, M.A. Dobrovolskaia, Nanoparticles and the immune system, Endocrinology 151 (2010) 458–465, https://doi.org/10.1210/en.2009-1082.

[17] R. Aebersold, M. Mann, Mass-spectrometric exploration of proteome structure and function, Nature 537 (2016) 347–355, https://doi.org/10.1038/nature19949.

[18] A. Shrestha, Z. Shi, K.G. Neoh, A. Kishen, Nanoparticulates for antibiofilm treatment and effect of aging on its antibacterial activity, J. Endod. 36 (2010) 1030–1035, https://doi.org/10.1016/j.joen.2010.02.008.

[19] F.C. Li, A. Kishen, Microtissue engineering root canal dentine with crosslinked biopolymeric nanoparticles for mechanical stabilization, Int. Endod. J. 51 (2018) 1171–1180, https://doi.org/10.1111/iej.12925.

[20] Z. Shi, K.G. Neoh, E.T. Kang, W. Wang, Antibacterial and mechanical properties of bone cement impregnated with chitosan nanoparticles, Biomaterials 27 (2006) 2440–2449, https://doi.org/10.1016/j.biomaterials.2005.11.036.

[21] D.G. Lin, D.J. Kenny, E.J. Barrett, P. Lekic, C.A. McCulloch, Storage conditions of avulsed teeth affect the phenotype of cultured human periodontal ligament cells, J. Periodontal. Res. 35 (2000) 42–50. https://www.ncbi.nlm.nih.gov/pubmed/10791708.

[22] M. Reifarth, S. Hoeppener, U.S. Schubert, Uptake and intracellular fate of engineered nanoparticles in mammalian cells: capabilities and limitations of transmission electron microscopy-polymer-based nanoparticles, Adv. Mater. 30 (2018), https://doi.org/10.1002/adma.201703704.

[23] J.E. Elias, S.P. Gygi, Target-decoy search strategy for increased confidence in large-scale protein identifications by mass spectrometry, Nat. Methods 4 (2007) 207–214, https://doi.org/10.1038/nmeth1019.

[24] E. Choudhary, C.K. Bullen, R. Goel, A.K. Singh, M. Praharaj, P. Thakur, R. Dhiman, W.R. Bishai, N. Agarwal, Relative and quantitative phosphoproteome analysis of macrophages in response to infection by virulent and avirulent, J. Proteome Res. 19 (2020) 2316–2336, https://doi.org/10.1021/acs.jproteome.9b00895.

[25] M. Ashburner, C.A. Ball, J.A. Blake, D. Botstein, H. Butler, J.M. Cherry, A.P. Davis, K. Dolinski, S.S. Dwight, J.T. Eppig, M.A. Harris, D.P. Hill, L. Issel-Tarver, A. Kasarskis, S. Lewis, J.C. Matese, J.E. Richardson, M. Ringwald, G.M. Rubin, G. Sherlock, Gene ontology: tool for the unification of biology. The Gene Ontology Consortium, Nat. Genet. 25 (2000) 25–29, https://doi.org/10.1038/75556.

[26] The Gene Ontology Consortium, The gene ontology resource: 20 years and still GOing strong, Nucleic Acids Res. 47 (2019) D330–D338, https://doi.org/10.1093/nar/gky1055.

[27] P.D. Thomas, M.J. Campbell, A. Kejariwal, H. Mi, B. Karlak, R. Daverman, K. Diemer, A. Muruganujan, A. Narechania, PANTHER: a library of protein families and subfamilies indexed by function, Genome Res. 13 (2003) 2129–2141, https://doi.org/10.1101/gr.772403.

[28] H. Li, S. Wei, Y. Fang, M. Li, X. Li, Z. Li, J. Zhang, G. Zhu, C. Li, L. Bi, G. Zhang, D. Wang, X.E. Zhang, Quantitative proteomic analysis of host responses triggered by Mycobacterium tuberculosis infection in human macrophage cells, Acta Biochim. Biophys. Sin. 49 (2017) 835–844, https://doi.org/10.1093/abbs/gmx080.

[29] J. Gould, GENE-E. [cited 2021 January, Available from, https://software.broadinstitute.org/GENE-E/.

[30] D. Szklarczyk, A.L. Gable, D. Lyon, A. Junge, S. Wyder, J. Huerta-Cepas, M. Simonovic, N.T. Doncheva, J.H. Morris, P. Bork, L.J. Jensen, C.V. Mering, TRING v11: protein-protein association networks with increased coverage, supporting functional discovery in genome-wide experimental datasets, Nucleic Acids Res. 47 (2019) D607–D613, https://doi.org/10.1093/nar/gky1131.

[31] X. Feng, W. Xu, Z. Li, W. Song, J. Ding, X. Chen, Immunomodulatory nanosystems, Adv. Sci. 6 (2019), 1900101, https://doi.org/10.1002/advs.201900101.

[32] L. Rueda-Gensini, J. Cifuentes, M.C. Castellanos, P.R. Puentes, J.A. Serna, C. Muñoz-Camargo, J.C. Cruz, Tailoring iron oxide nanoparticles for efficient cellular internalization and endosomal escape, Nanomaterials (2020) 10, https://doi.org/10.3390/nano10091816.

[33] L.Q. Jiang, T.Y. Wang, T.J. Webster, H.J. Duan, J.Y. Qiu, Z.M. Zhao, X.X. Yin, C. L. Zheng, Intracellular disposition of chitosan nanoparticles in macrophages: intracellular uptake, exocytosis, and intercellular transport, Int. J. Nanomed. 12 (2017) 6383–6398, https://doi.org/10.2147/IJN.S142060.

[34] N.R. Patel, M. Bole, C. Chen, C.C. Hardin, A.T. Kho, J. Mih, L. Deng, J. Butler, D. Tschumperlin, J.J. Fredberg, R. Krishnan, H. Koziel, Cell elasticity determines macrophage function, PLoS One 7 (2012), e41024, https://doi.org/10.1371/journal.pone.0041024.

[35] S. Takashiba, K. Naruishi, Y. Murayama, Perspective of cytokine regulation for periodontal treatment: fibroblast biology, J. Periodontol. 74 (2003) 103–110, https://doi.org/10.1902/jop.2003.74.1.103.

[36] J.C. Baumgartner, W.A. Falkler, Bacteria in the apical 5 mm of infected root canals, J. Endod. 17 (1991) 380–383, https://doi.org/10.1016/s0099-2399(06)81989-8.

[37] G. Sundqvist, D. Figdor, S. Persson, U. Sjögren, Microbiologic analysis of teeth with failed endodontic treatment and the outcome of conservative re-treatment, Oral Surg. Oral Med. Oral Pathol. Endod. 85 (1998) 86–93, https://doi.org/10.1016/s1079-2104(98)90404-8.

[38] L.E. Chavez de Paz, L. Chávez de Paz, Redefining the persistent infection in root canals: possible role of biofilm communities, J. Endod. 33 (2007) 652–662, https://doi.org/10.1016/j.joen.2006.11.004.

[39] C. Zhang, J. Du, Z. Peng, Correlation between Enterococcus faecalis and persistent intraradicular infection compared with primary intraradicular infection: a systematic review, J. Endod. 41 (2015) 1207–1213, https://doi.org/10.1016/j.joen.2015.04.008.

[40] N. Pappireddi, L. Martin, M. Wühr, A review on quantitative multiplexed proteomics, Chembiochem 20 (2019) 1210–1224, https://doi.org/10.1002/cbic.201800650.

[41] Y. Liu, A. Beyer, R. Aebersold, On the dependency of cellular protein levels on mRNA abundance, Cell 165 (2016) 535–550, https://doi.org/10.1016/j.cell.2016.03.014.

[42] N. Rauniyar, Parallel reaction monitoring: a targeted experiment performed using high resolution and high mass accuracy mass spectrometry, Int. J. Mol. Sci. 16 (2015) 28566–28581, https://doi.org/10.3390/ijms161226120.

[43] A. Batista-Gonzalez, R. Vidal, A. Criollo, L.J. Carreño, New insights on the role of lipid metabolism in the metabolic reprogramming of macrophages, Front. Immunol. 10 (2019) 2993, https://doi.org/10.3389/fimmu.2019.02993.

[44] A. Viola, F. Munari, R. Sánchez-Rodríguez, T. Scolaro, A. Castegna, The metabolic signature of macrophage responses, Front. Immunol. 10 (2019) 1462, https://doi.org/10.3389/fimmu.2019.01462.

[45] R. Madan, R. Rastogi, S. Parashuraman, A. Mukhopadhyay, Salmonella acquires lysosome-associated membrane protein 1 (LAMP1) on phagosomes from Golgi via SipC protein-mediated recruitment of host Syntaxin6, J. Biol. Chem. 287 (2012) 5574–5587, https://doi.org/10.1074/jbc.M111.286120.

[46] F.R. Ribeiro-Santos, G.G.D. Silva, I.B.F. Petean, M.F.M. Arnez, L.A.B.D. Silva, L. H. Faccioli, F.W.G. Paula-Silva, Periapical bone response to bacterial lipopolysaccharide is shifted upon cyclooxygenase blockage, J. Appl. Oral Sci. 27 (2019), e20180641, https://doi.org/10.1590/1678-7757-2018-0641.

[47] S.S. Bohlson, S.D. O'Conner, H.J. Hulsebus, M.M. Ho, D.A. Fraser, Complement, c1q, and c1q-related molecules regulate macrophage polarization, Front. Immunol. 5 (2014) 402, https://doi.org/10.3389/fimmu.2014.00402.

[48] F. Cavalla, C. Biguetti, S. Jain, C. Johnson, A. Letra, G.P. Garlet, R.M. Silva, Proteomic profiling and differential messenger RNA expression correlate HSP27 and serpin family B member 1 to apical periodontitis outcomes, J. Endod. 43 (2017) 1486–1493, https://doi.org/10.1016/j.joen.2017.03.014.

[49] A. Torriglia, E. Martin, I. Jaadane, The hidden side of SERPINB1/Leukocyte Elastase Inhibitor, Semin. Cell Dev. Biol. 62 (2017) 178–186, https://doi.org/10.1016/j.semcdb.2016.07.010.

[50] Y.J. Choi, S. Kim, Y. Choi, T.B. Nielsen, J. Yan, A. Lu, J. Ruan, H.R. Lee, H. Wu, B. Spellberg, J.U. Jung, SERPINB1-mediated checkpoint of inflammatory caspase activation, Nat. Immunol. 20 (2019) 276–287, https://doi.org/10.1038/s41590-018-0303-z.

[51] S.S. Burgener, N.G.F. Leborgne, S.J. Snipas, G.S. Salvesen, P.I. Bird, C. Benarafa, Cathepsin G inhibition by Serpinb1 and Serpinb6 prevents programmed necrosis in neutrophils and monocytes and reduces GSDMD-driven inflammation, Cell Rep. 27 (2019) 3646–3656, https://doi.org/10.1016/j.celrep.2019.05.065, e5.

[52] S. Toyokuni, I. Yanatori, Y. Kong, H. Zheng, Y. Motooka, L. Jiang, Ferroptosis at the crossroads of infection, aging and cancer, Cancer Sci. 111 (2020) 2665–2671, https://doi.org/10.1111/cas.14496.

[53] H.Y. Tan, N. Wang, S. Li, M. Hong, X. Wang, Y. Feng, The reactive oxygen species in macrophage polarization: reflecting its dual role in progression and treatment of human diseases, Oxid. Med. Cell. Longev. 2016 (2016), 2795090, https://doi.org/10.1155/2016/2795090.

[54] H. Feng, Z. Li, J. Du, J. Sun, W. Feng, D. Li, S. Liu, W. Wang, H. Liu, N. Amizuka, M. Li, Dual function of peroxiredoxin I in lipopolysaccharide-induced osteoblast

[55] S.G. Rhee, S.W. Kang, T.S. Chang, W. Jeong, K. Kim Peroxiredoxin, A novel family of peroxidases, IUBMB Life 52 (2001) 35–41, https://doi.org/10.1080/15216540252774748.

[56] P. Hernandez-Rios, P.J. Pussinen, R. Vernal, M. Hernandez, Oxidative stress in the local and systemic events of apical periodontitis, Front. Physiol. 8 (2017) 869, https://doi.org/10.3389/fphys.2017.00869.

[57] I. Graunaite, G. Lodiene, V. Maciulskiene, Pathogenesis of apical periodontitis: a literature review, J. Oral Maxillofac. Res. 2 (2012) e1, https://doi.org/10.5037/jomr.2011.2401.

[58] V. Audrito, S. Serra, F. Brusa, F. Mazzola, F. Arruga, T. Vaisitti, M. Coscia, R. Maffei, D. Rossi, T. Wang, G. Inghirami, M. Rizzi, G. Gaidano, J.G. Garcia, C. Wolberger, N. Raffaelli, S. Deaglio, Extracellular nicotinamide phosphoribosyltransferase (NAMPT) promotes M2 macrophage polarization in chronic lymphocytic leukemia, Blood 125 (2015) 111–123, https://doi.org/10.1182/blood-2014-07-589069.

[59] C. Travelli, G. Colombo, S. Mola, A.A. Genazzani, C. Porta NAMPT, A pleiotropic modulator of monocytes and macrophages, Pharmacol. Res. 135 (2018) 25–36, https://doi.org/10.1016/j.phrs.2018.06.022.

[60] P. Samara, K. Ioannou, O.E. Tsitsilonis, Prothymosin alpha and immune responses: are we close to potential clinical applications? Vitam. Horm. 102 (2016) 179–207, https://doi.org/10.1016/bs.vh.2016.04.008.

[61] P. Stashenko, Role of immune cytokines in the pathogenesis of periapical lesions, Endod. Dent. Traumatol. 6 (1990) 89–96. https://www.ncbi.nlm.nih.gov/pubmed/2079017.

[62] S. Ran, J. Huang, B. Liu, S. Gu, W. Jiang, J. Liang, Enterococcus Faecalis activates NLRP3 inflammasomes leading to increased interleukin-1 beta secretion and pyroptosis of THP-1 macrophages, Microb. Pathog. 154 (2021) 104761, https://doi.org/10.1016/j.micpath.2021.104761.

[63] H.H. Yang, H.K. Jun, Y.J. Jung, B.K. Choi, Enterococcus faecalis activates caspase-1 leading to increased interleukin-1 beta secretion in macrophages, J. Endod. 40 (2014) 1587–1592, https://doi.org/10.1016/j.joen.2014.06.015.

[64] P.J. Murray, T.A. Wynn, Protective and pathogenic functions of macrophage subsets, Nat. Rev. Immunol. 11 (2011) 723–737, https://doi.org/10.1038/nri3073.

[65] J.E. Feugate, Q. Li, L. Wong, M. Martins-Green, The cxc chemokine cCAF stimulates differentiation of fibroblasts into myofibroblasts and accelerates wound closure, J. Cell Biol. 156 (2002) 161–172, https://doi.org/10.1083/jcb.200103062.

[66] G.T. Huang, M. Do, M. Wingard, J.S. Park, N. Chugal, Effect of interleukin-6 deficiency on the formation of periapical lesions after pulp exposure in mice, Oral Surg. Oral Med. Oral Pathol. Oral Radiol. Endod. 92 (2001) 83–88, https://doi.org/10.1067/moe.2001.115025.

[67] L.R. Luckett-Chastain, R.M. Gallucci, Interleukin (IL)-6 modulates transforming growth factor-beta expression in skin and dermal fibroblasts from IL-6-deficient mice, Br. J. Dermatol. 161 (2009) 237–248, https://doi.org/10.1111/j.1365-2133.2009.09215.x.

[68] Q.Z. Zhang, W.R. Su, S.H. Shi, P. Wilder-Smith, A.P. Xiang, A. Wong, A.L. Nguyen, C.W. Kwon, A.D. Le, Human gingiva-derived mesenchymal stem cells elicit polarization of m2 macrophages and enhance cutaneous wound healing, Stem Cell. 28 (2010) 1856–1868, https://doi.org/10.1002/stem.503.

apoptosis via reactive oxygen species and the apoptosis signal-regulating kinase 1 signaling pathway, Cell Death Dis. 4 (2018) 47, https://doi.org/10.1038/s41420-018-0050-9.